THE JOURNAL OF PHYSICAL CHEMISTRY B LETTERS

2006, *110,* 4514−4518
Published on Web 02/17/2006

Correlation between Volume Change and Cell Voltage Variation with Composition for Lithium Intercalated Amorphous Films

Germà Garcia-Belmonte,* Jorge García-Cañadas, and Juan Bisquert

Departament de Ciències Experimentals, Universitat Jaume I, E-12071 Castelló, Spain

Received: January 10, 2006; In Final Form: February 3, 2006

Interactions between the intercalant and the host have been studied in homogeneous amorphous Li_xWO_3 prepared by electron beam evaporation, using electrochemical experiments with films of different thickness (100−400 nm). We have related the intercalation thermodynamics, described previously by us [*Solid State Ionics* **2005**, *176*, 1701] with other models that take into account film volume dilatation along the intercalation. A distinct behavior of cell voltage variation with composition and volume change is observed for the thinnest (100 nm) films: cell voltage follows ideal insertion thermodynamics and no deformation was detected using profilometry techniques. In contrast, thicker films exhibited both volume changes and, correspondingly, cell voltage departs from ideality due to contributions to the chemical potential arising from elastic distortions of the host matrix.

1. Introduction

One of the most challenging issues in the development of devices based on lithium intercalation materials is taking control over structural changes and deformations produced by lithium insertion/removal. In many cases, mechanical strain generated in intercalation/deintercalation cycles induces structural as well as volume changes of the electrode material, leading to fracturing, cracking, and even crumbling and, thereby, to electrode irreversibility upon cycling. As recently stressed,[1] promising research is in course exploring the advantages of nanostructured materials for storage devices. Together with beneficial effects associated with the rate improvement due to shortening in path length for electronic and ionic transport, it has been proposed that size confinement of nanocomposites is also able to suppress particle deformation and reduce fracturing.[2] Improvement has been reported of silicon-based anode materials made up of nanosized silicon particles embedded in a sol−gel graphite matrix[3] or Sn nanodots dispersed in silicon electrodes synthesized by co-sputtering.[4]

In parallel with innovation in nanostructured materials, it is known that amorphous intercalation materials are potentially useful as electroactive electrodes for lithium batteries, supercapacitors, and electrochromic windows.[5−8] The intrinsic structural disorder of these compounds is likely to lie behind the rather distinct electrochemical properties with respect to their crystalline counterparts. It has been suggested that the amorphous structure can accommodate smoothly the distortion caused by the guest species without producing a macroscopic phase transition.[8] Accordingly, the combination of nano- and amorphous-structuring has been recently explored for precluding deformation of electrode material. For instance, nanosized amorphous iron oxyhydroxide-based electrodes exhibited improved capacity retention upon cycling and excellent rate performance.[9] An amorphous TiO_2 nanopowder-based electrode also showed enhanced features.[10]

Besides efforts addressed to technological improvement, there is also interest in stating experimentally the relation between volume change undergone by the electrode material and the underlying intercalation thermodynamics. The host−guest interaction responsible for the electrode mechanical distortion or phase separation has been examined, particularly in crystalline and layered host matrixes.[11,12] Analysis of the thermodynamics of lithium and sodium intercalation into crystalline WO_3 showed[13] the intercalation-induced restructuring of the host lattice. Self-stress effect is also a widely discussed issue in hydrogen intercalation into metals and alloys.[14,15] The case of a more complex host matrix such as that of an entirely amorphous structure has been theoretically addressed by Vakarin.[16]

Very recently, we proposed[17,18] a phenomenological approach for interpreting the cell voltage variation with the amount of inserted ions by regarding contributions to the chemical potential of Li^+ inside the amorphous film caused by host distortions. In this approach, the chemical potential takes the form[18]

$$\mu = E_0 + (1+\eta)Gx^{\eta} + \beta^{-1}\ln\frac{x}{1-x} \qquad (1)$$

In this equation, the first term E_0 corresponds to a constant energy level, the second one $(1 + \eta)Gx^{\eta}$ relates to the dependence of the intercalant−host interaction with the insertion level. For $G > 0$, additional energy is needed to deform the host. A power-law dependence with composition with $\eta < 1$ was reported.[17] The last summand accounts for the entropic term ($\beta^{-1} = k_BT$ is the thermal energy). The working electrode potential U is related to the variation of the chemical potential

* Corresponding author. Tel.: +34 964 728023. Fax: +34 964 728066 E-mail: garciag@uji.es.

10.1021/jp060171b CCC: $33.50

with composition $U = -(\mu - \mu_{ref})/e$, where e stands for the positive elementary charge. This view then highlights contributions to the chemical potential arising from distortions of the host matrix caused by the intercalation process itself.[19] A different approach which is quite reasonable for disordered materials considers a wide distribution of site energies.[6,20] This is a model of noninteracting ions randomly occupying available sites. Gaussian site distributions yielded good fits to the potential−composition curves of a-WO_3.[6] On the basis of simple consideration, the distribution of sites model should predict an increase in the ionic mobility as the occupancy of deeper sites with increasing x proceeds. However, we have recently reported the opposite behavior for the films used in this study.[5]

With the aim of gaining further insight into the thermodynamics of lithium intercalation, we have studied the electrochemical and volume-change response of thin-film amorphous WO_3 electrodes, with thicknesses ranging from 100 nm up to 400 nm. We observed the distinct behavior of cell voltage variation with composition and volume change for the thinnest films (100 nm thick), in which the cell voltage follows ideal insertion thermodynamics and no deformation was detected using profilometry techniques. In contrast, thicker films exhibited both volume changes and, correspondingly, cell voltage departures from ideality due to contributions to the chemical potential arising from distortions of the host matrix. The host−guest interaction parameter G was found to be dependent on the film thickness, being equal to zero (ideal thermodynamics) for thinner (100 nm) films. In this work, eq 1 is related to the thermodynamic function first introduced by Vakarin[21,22] showing that the parameter G can be interpreted in terms of volume change undergone by the films. Volume changes measured experimentally are coherent with the expansion values extracted from eq 1.

2. Results

All samples in this work, WO_3 onto indium−tin oxide (ITO) substrates, were deposited by electron beam evaporation using the procedure described elsewhere.[23] The thickness of the samples was varied within the range of 100−400 nm by adjusting the deposition time and later confirmed by profilometry techniques (Dektak 6M profiler from Veeco). Samples exhibited an X-ray amorphous structure, as verified using a Bruker CCD-Smart difractometer. Electrochemical measurements (chronopotentiometry at a constant current of 1 μA cm^{-2} to ensure quasiequilibrium conditions) were carried out in a shielded two-electrode cell mounted in a glovebox. Samples of a-WO_3 deposited onto ITO substrates were the working electrodes immersed in a solution of 0.5 M $LiClO_4$ in propylene carbonate. A lithium foil was used as both the counter and reference electrodes. Reversibility upon lithium insertion/removal was carefully checked by cyclic voltammetry[23] and optical transmittance. It was observed that submitting the films to $x > 0.6$ values caused irreversible changes in the voltammetric response, as reported by other authors for similar films.[24] Films for volume expansion measurements were submitted to constant current intercalation (1 μA cm^{-2}) till a doping level equal to $x = 0.4$ was reached. Then the electrodes were removed from the electrochemical cell, dried in air, and placed on the profilometer (confocal imaging profiler Sensofar PLμ) sample holder.

As we will next discuss, stress energy upon film deformation introduces additional terms into the thermodynamic function of lithium intercalation. It is therefore important to determine mechanical parameters such as the Young modulus E of the a-WO_3 films. This was measured using nanoindentation techniques (Nano Indenter XP from MTS) with continuous stiffness measurement at $x = 0$, i.e., before film expansion. The Young modulus was $E \approx 50$ GPa, with slight variations by varying the film thickness (see Table 1). This technique could not be used to measure the E value for the thinnest film.

TABLE 1: Fitting Parameters Resulting by Using the Variation of the Chemical Capacitance with Composition of Eq 3[a]

film thickness (nm)	N (10^{21}cm^{-3})	G (eV)	η	E (GPa)
100	6.2 (1.3)	<0.001		
200	4.8 (1.0)	0.058 (0.03)	0.59 (0.02)	51 (10)
300	8.6 (1.1)	0.283 (0.04)	0.51 (0.01)	50 (7)
400	7.8 (1.0)	0.354 (0.01)	0.50 (0.01)	56 (7)

[a] Young modulus E obtained by averaging from 25 nanoindentations.

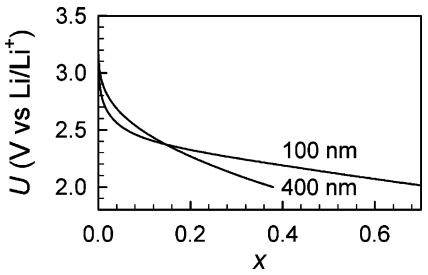

Figure 1. a-Li_xWO_3 electrode potential as a function of the composition (molar fraction) x obtained under constant current (1 μA cm^{-2}) Li^+ insertion in a solution 0.5 M $LiClO_4$ in propylene carbonate for two different film thickness indicated in each curve.

From titration experiments shown in Figure 1, the chemical capacitance (per unit volume) was calculated using[25,26]

$$C_\mu = C_0 \frac{\partial x}{\partial(\beta\mu)} \tag{2}$$

where $C_0 = \beta e^2 N$ is a constant approximately equal to 20 kF cm^{-3} for these films. N stands for the number density of the host atoms. Variations of $C_\mu(x)$ are shown in Figure 2a in a log−log representation that highlights asymptotic dependences in the intercalation level within $10^{-3} < x < 0.6$. By examining Figure 2a, one can observe a clear change of the asymptotic slope m of the capacitance with x under variation of the film thickness. The slope tends to 1 as the film thickness is reduced and reaches $m \approx 0.65$ for the thickest film as stated in previous works.[17,18]

Chemical capacitance results from combining eqs 1 and 2 as[18]

$$C_\mu = C_0\left[\eta(1+\eta)\beta G x^{\eta-1} + \frac{1}{x(1-x)}\right]^{-1} \tag{3}$$

We have used eq 3 in order to fit the behavior exhibited by the chemical capacitance (see Figure 2 for a comparison between fitting and experimental curves). Excellent fits were obtained. For the thinnest (100 nm) film, the intercalant−host interaction term G is not detectable so that the system behaves like an ideal noninteracting lattice gas in which entropic contributions play the determining role. In this case, a power-law relationship as $C_\mu \propto x$ for $x \ll 1$ is obeyed. As the thickness is increased, G becomes larger which modifies the asymptotic behavior of the chemical capacitance (see Figure 2a). The exponent of the intercalant−host interaction term resulted in $\eta \approx 0.5$, and N laid within the range of 10^{22} cm^{-3}. All fitting parameters are summarized in Table 1.

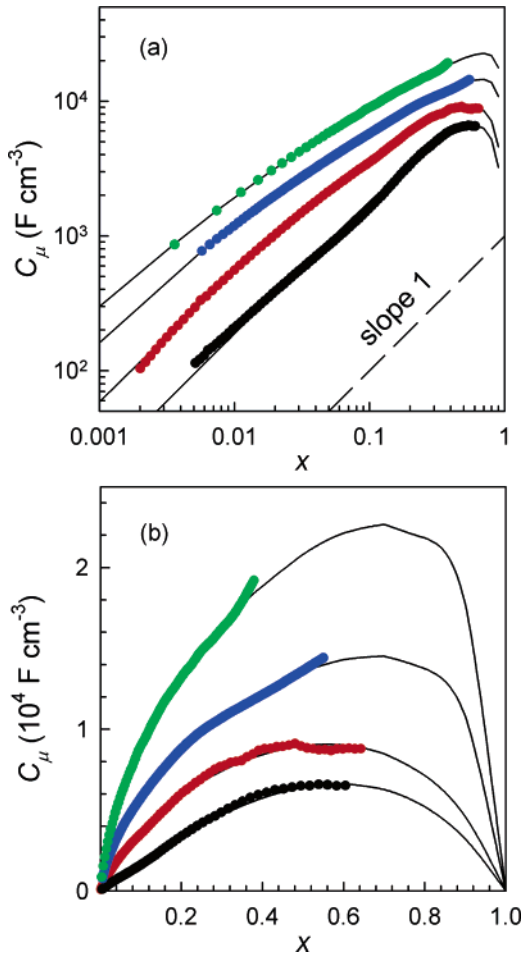

Figure 2. Chemical (equilibrium) film capacitance C_μ as a function of the composition (molar fraction) x for film thickness (in nm): (black) 100, (red) 200, (blue) 300, and (green) 400. Fine solid lines correspond to fits using eq 3. Capacitance is multiplied by 2, 4, and 8 for thickness 200, 300, and 400 nm, respectively, to improve the clarity of the graph. (a) log−log representation highlighting the asymptotic behavior at $x \ll 1$. A reference dashed line of slope 1 is shown. (b) Linear representation showing general response.

The relative volume changes at $x = 0.4$ of a set of a-WO_3 films with different thicknesses were measured with a confocal imaging profiler. Figure 3 corresponds to a topographic representation of the height reached by the outer surface of the film. The image for the 200 nm thick film, which spreads over an area of 637 × 477 μm^2, clearly shows the bordering limit of the intercalated part (left side of Figure 3a) and the flat surface corresponding to the nonintercalated film region. The expansion is observed to yield a highly rough surface in the intercalated part. The software of the instrument allows the average volume expansion to be determined by means of proper image algorithms. All films showed similar patterns, relative volume changes near 10% on average (see Figure 4), except for the 100 nm-thick samples (Figure 3b) which presented no expansion at all (same scanned area), in good agreement with findings resulting from electrochemical measurements ($G = 0$).

3. Discussion

To correlate electrochemical and topographic measurements, we need to extract information related to film expansion from the fitting parameters obtained in analyzing the chemical capacitance response in eq 3. In previous reports,[21,22] it has already been considered that volume changes upon intercalation

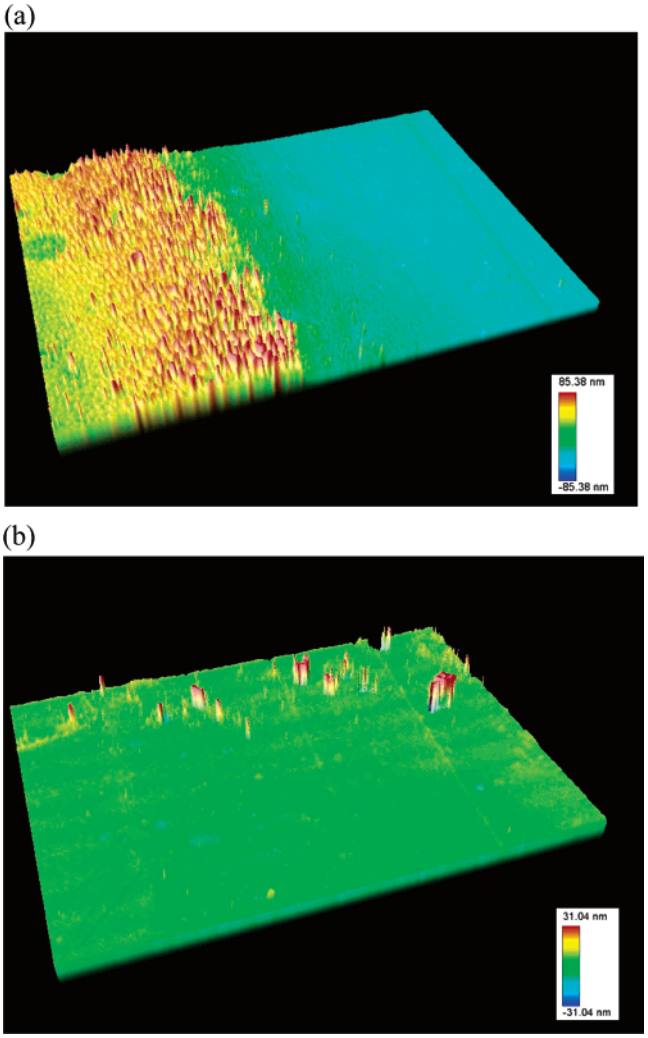

Figure 3. Topography of two a-WO_3 films of 200 (a) and 100 nm (b) of the border between a nonintercalated area (right part of the image) and an intercalated one (left part of the image) at $x = 0.4$. Volume change is not observed for 100 nm thick samples. Scanned area is 637 × 477 μm^2.

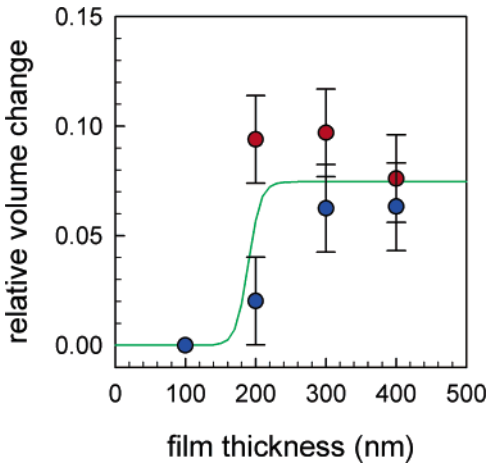

Figure 4. Relative volume change comparison at $x = 0.4$ between values measured by direct profilometry measurements (red dot) and using fitting parameters of the chemical capacitance response with composition (Table 1) and eq 10 (blue dots). Solid line is a fitting made from all points.

have an influence on the cell voltage. In this model, it is assumed that there is an additional term to the host−guest free energy resulting from the elastic interaction[21]

$$F_{el}(x) = \frac{1}{2}\Lambda\epsilon(x)^2 - \sigma(x)\epsilon(x) \quad (4)$$

Λ represents an effective, concentration-independent elastic constant, $\epsilon(x)$ stands for the strain the film undergoes upon guest intercalation, and finally $\sigma(x)$ corresponds to loading stress resulting from other mechanisms different than dilatation. The total stress $S(x) = dF_{el}/d\epsilon$ conveys then two terms. The internal, or self-stress, $\Lambda\epsilon(x)$ accounts for the host reaction to the intercalant insertion and the stress resulting from the loading procedure, $\sigma(x)$.

The chemical potential is given by the concentration derivative of the total free energy, which in addition to the term derived from simple lattice gas statistics $\mu_0 = E_0 + \beta^{-1}\ln(x/1-x)$ should contain the elastic contribution[21]

$$\mu = \mu_0 + \Lambda S(x)\frac{d\epsilon(x)}{dx} - \frac{d\sigma(x)}{dx}\epsilon(x) \quad (5)$$

The second term involves the so-called chemical expansion coefficient $d\epsilon/dx$.

With the aim of relating eq 5 with the experimentally obtained function for the chemical potential of eq 1, we will assume that all of the stress applied to the sample by the intercalation process is transformed in elastic energy by deforming the lattice. This corresponds to vanishing loading stress $\sigma(x) = 0$, as in the case of unclamped films.[22] One readily arrives at the following expression for the chemical potential:

$$\mu = E_0 + \beta^{-1}\ln\frac{x}{1-x} + \Lambda\delta^2 p(x)\frac{dp(x)}{dx} \quad (6)$$

where $\delta = [V(1) - V(0)]/V(0)$ is the relative volume variation and $p(x) = [V(x) - V(0)]/[V(1) - V(0)]$ is the modulating fraction, in such a way that $\epsilon(x) = \delta p(x)$. To connect this expression with our model (eq 1), we adopt the following identifications:

$$\frac{(1+\eta)x^\eta}{\alpha} = p(x)\frac{dp(x)}{dx} \quad (7)$$

$$\alpha G = \Lambda\delta^2 \quad (8)$$

with $\alpha = 2$ being a proportionality constant, which results from the limiting constraints $p(0) = 0$ and $p(1) = 1$. After integration of eq 7, it is found that the expansion fraction obeys a power-law of concentration

$$p(x) = x^{(1+\eta)/2} \quad (9)$$

Equation 9 implies that the film expansion exhibits a rather smooth, sublinear response presumably caused by the amorphous structure of the films that steeply accommodates the deformation. Since the exponent in eq 9 results in $(1+\eta)/2 \approx 0.75$, one obtains a response near the linear Vegard's law.[27]

The effective elastic constant appearing in eq 8 can be readily written in terms of the Young modulus of the films, $\Lambda = eE/N$, and therefore, one arrives at an expression for determining relative expansions at full intercalation

$$\delta = \left(\frac{2GN}{eE}\right)^{1/2} \quad (10)$$

Values of volume changes at $x = 0.4$ can be simply obtained by doing the product $\delta p(0.4)$.

By applying eqs 10 and 9, the parameters obtained from chemical capacitance fitting, along with the elastic constant E measured, we have an alternative way for determining film expansion. These values are compared with those obtained through profilometry measurements (Figure 4).

By examining Figure 4 one can realize that both measurements (electrochemical and profilometric) result in film volume change around 10% in the case of thicker films (300−400 nm). The agreement is even excellent for the thinnest films (100 nm) for which no expansion is detected and, accordingly, no deviation from the simple lattice gas model is observed. Between these two extreme limits, there must be a transition thickness around 200 nm at which the films do not undergo full expansion. A sharp transition region can explain the difference in volume changes resulting from both techniques for 200 nm thick films.

It is worth noting the clearly distinct intercalation behavior reported for 100 nm-thick films in comparison with thicker films. The fact that thinnest films do not exhibit volume changes points to the occurrence of a particular intercalation mechanism somehow governed by the reduction in the layer size. It may be interesting to speculate about the possible origin of such change in the intercalation mechanism. It is broadly accepted that charge storage in bulk materials occurs by homogeneous intercalation of electrons and ions into the host electrode. Yet an alternative charge storage mode has recently been suggested, derived from the charge separation at interfacial boundaries. Jamnik and Maier[28] have specifically addressed nanosize effects in lithium intercalation materials. For semiconductor materials in contact with a metal (or quasimetallic material like ITO), an electron depletion layer is formed with a length depending on specific parameters of the contact but usually shorter than 200 nm. It has then been suggested[28] that a purely electron insertion, compensated by ions distributed near the surface of depleted nanoparticles, is able to reach chemical capacitance values as large as those expected for homogeneous, bulk intercalation. The situation resembles that encountered in electron storage in porous TiO_2 layers made up of particles of nanometer size.[29] Other possibilities cannot be completely discarded: the assumption we have adopted in deriving eq 6 that the loading stress $\sigma(x)$ is safely negligible is perhaps a simplification of the real stress field built at the ITO/WO_3 interface. Differences in the amorphous structure (free volume) may also be behind the experimental observations. Further research is needed aiming to interpret the distinct response reported for thinner *a*-WO_3 films in terms of such recently introduced intercalation mechanisms.[28] A full analysis lies however outside the scope of this work.

4. Conclusion

A comparison of the thermodynamic function (eq 1) with the previous model which describes host lattice expansions upon intercalation (eq 6) led us to calculate volume change produced in the films. Using simple chronopotenciometry measurements and the resulting chemical capacitance analyzed from eq 3, the volume change experienced by the film along intercalation can be calculated, which are reported to be in good agreement with direct profilometry data. We can conclude that film expansion and cell voltage are both determined by means of the underlying intercalation thermodynamics.

We have also observed a distinct intercalation behavior for the thinnest layers. This fact informs us about a size effect able to preclude volume change of the films and, consequently, to avoid capacity losses produced after host expansion/compression upon lithium insertion/removal.

Acknowledgment. This work was supported by Generalitat Valenciana (Spain) under Project GV04B-028. Use of SCIC-UJI facilities and nanoindentation techniques from LTM-Centre Tecnològic de Manresa are acknowledged.

References and Notes

(1) Aricò, A. S.; Bruce, P.; Scrosati, B.; Tarascon, J.-M.; van Schalkwijk, W. *Nat. Mater.* **2005**, *4*, 366.
(2) Ryu, J. H.; Kim, J. W.; Sung, Y.; Oh, S. M. *Electrochem. Solid State Lett.* **2004**, *7*, A306.
(3) Niu, J.; Lee, J. Y. *Electrochem. Solid State Lett.* **2002**, *5*, A107.
(4) Ahn, H.; Kim, Y.; Park, K.; Seong, T. *Chem. Commun.* **2005**, 43.
(5) García-Cañadas, J.; Fabregat-Santiago, F.; Porqueras, I.; Person, C.; Bisquert, J.; Garcia-Belmonte, G. *Solid State Ionics* **2004**, *175*, 521.
(6) Strömme, M. *Phys. Rev. B* **1998**, *58*, 11015.
(7) Fu, Z. W.; Huang, F.; Chu, Y. Q.; Zhang, Y.; Qin, Q. Z. *J. Electrochem. Soc.* **2003**, *150*, A776.
(8) Kim, J.; Manthiran, A. *Nature* **1997**, *390*, 265.
(9) Jain, G.; Capozzi, C. J.; Xu, J. J. *J. Electrochem. Soc.* **2003**, *150*, A806.
(10) Furukawa, H.; Hibino, M.; Honma, I. *J. Electrochem. Soc.* **2004**, *151*, A527.
(11) Fischer, J. E.; Kim, H. J. *Phys. Rev. B* **1987**, *35*, 3295.
(12) Vakarin, E. V.; Badiali, J. P.; Levi, M. D.; Aurbach, D. *Phys. Rev. B* **2001**, *63*, 014304.
(13) Vakarin, E. V.; Badiali, J. P. *Electrochim. Acta* **2001**, *46*, 4151.
(14) Legawiec, B.; Zoltowski, P. *J. Phys. Chem. B* **2002**, *106*, 4933.
(15) Gabrielli, C.; Grand, P. P.; Lasia, A.; Perrot, P. *J. Electrochem. Soc.* **2004**, *155*, A1925.
(16) Vakarin, E. V.; Badiali, J. P. *Electrochim. Acta* **2005**, *50*, 1719.
(17) Garcia-Belmonte, G.; Vikhrenko, V. S.; García-Cañadas, J.; Bisquert, J. *Solid State Ionics* **2004**, *170*, 123.
(18) García-Cañadas, J.; Garcia-Belmonte, G.; Bisquert, J.; Porqueras, I.; Person, C. *Solid State Ionics* **2005**, *176*, 1701.
(19) In fact, the chemical potential in eq 1 should contain contributions from ions and electrons. The strict separation is not always possible because of interactions terms between both. We can however assume that at high enough intercalation levels (high electronic conductivity) the electronic part is a constant assimilated into E_0.
(20) Kudo, T.; Hibino, M. *Solid State Ionics* **1996**, *84*, 65.
(21) Vakarin, E. V.; Badiali, J. P. *J. Phys. Chem. B* **2002**, *106*, 7721.
(22) Vakarin, E. V.; Badiali, J. P. *Solid State Ionics* **2004**, *171*, 261.
(23) García-Cañadas, J.; Mora-Seró, I.; Fabregat-Santiago, F.; Bisquert, J.; Garcia-Belmonte, G. *J. Electroanal. Chem.* **2004**, *565*, 329.
(24) Lee, S. H.; Seong, M. J.; Cheong, H. M.; Ozkan, E.; Tracy, E. C.; Deb, S. K. *Solid State Ionics* **2003**, *156*, 447.
(25) Jamnik, J.; Maier, J. *Phys. Chem. Chem. Phys.* **2001**, *3*, 1668.
(26) Bisquert, J. *Electrochim. Acta* **2002**, *47*, 2435.
(27) Lee, S.; Miyazaki, H.; Mahanti, S. D.; Solin, S. A. *Phys. Rev. Lett.* **1989**, *62*, 3066.
(28) Jamnik, J.; Maier, J. *Phys. Chem. Chem. Phys.* **2003**, *5*, 5215.
(29) Fabregat-Santiago, F.; Mora-Seró, I.; Garcia-Belmonte, G.; Bisquert, J. *J. Phys. Chem. B* **2003**, *107*, 758.